HOSTED BY
ELSEVIER
Available online at www.sciencedirect.com
ScienceDirect
Soils and Foundations 64 (2024) 101438
SOILS AND FOUNDATIONS
www.elsevier.com/locate/sandf

Technical Paper

Triaxial testing response of compacted iron ore tailings considering a broad spectrum of confining pressures

João Paulo Sousa Silva [a], Ana Luisa Cezar Rissoli [a], Pedro Pazzoto Cacciari [a,b], António Joaquim Pereira Viana da Fonseca [c], Hugo Carlos Scheuermann Filho [d], Alexia Cindy Wagner [d], João Vítor de Azambuja Carvalho [d], Lucas Festugato [d], Nilo Cesar Consoli [d,*]

[a] *Exploration and Mineral Projects - Mineral Development Centre, VALE S.A, Santa Luzia, MG 33040-900, Brazil*
[b] *Department of Civil, Geological and Mining Engineering, Polytechnique Montreal, Quebec H3C 3A7, Canada*
[c] *Faculty of Engineering, Universidade do Porto, Porto, Portugal*
[d] *Graduate Program in Civil Engineering, Universidade Federal do Rio Grande do Sul, Porto Alegre, RS 90035-190, Brazil*

Received 20 March 2023; received in revised form 16 January 2024; accepted 1 February 2024
Available online 16 February 2024

Abstract

The filtered tailings disposal (dry stacking) up to 300 m high is an alternative to overcome the drawbacks related to the slurry tailings storage in large impoundments as it is safer and demands smaller portions of the existing landform. Even so, the understanding of the denser and dewatered material response over a broad range of confining pressures is essential to safely design tall dry stacking tailings facilities. Accordingly, the present research assesses the mechanical behavior of compacted iron ore tailings through triaxial tests. A series of compression and extension drained and undrained triaxial tests were conducted over a wide spectrum of confinements (σ'_3 ranging from 75 to 8,000 kPa) to check possible particle breakage occurrence and effects. The influence of the initial density due to compaction was, as well, evaluated since the tests were performed using specimens molded at distinct dry unit weight values. The results were analyzed in the light of the critical state soil mechanics and have indicated the existence of a curvilinear critical state line in the v: log p' plane. Small particle breakage has occurred and can be associated with reduction in surface roughness, breakage of asperities, and reduction in particle angularity. Moreover, a tendency for static liquefaction was observed amongst the loosest specimens sheared under the lowest confining levels.

Keywords: Tailings; Iron ore tailings; Tailings dam; Filtered tailings disposal; Dry stacking; Critical state soil mechanics; Static liquefaction

1. Introduction

Tailings are the remains of ore extraction and processing, being mainly composed of crushed rock fines, chemicals, and water (Kossoff et al., 2014; Xiaolong et al., 2021). This mixture of fine suspended materials is typically poured into vast impoundments, the tailings dams. Such structures, schematically depicted in Fig. 1, can be gradually expanded as the demand for storage space increases. There are cases that the raising dam is founded above the

* Corresponding author.
E-mail addresses: joao.paulo.silva@vale.com (J.P.S. Silva), ana.rissoli@vale.com (A.L.C. Rissoli), pedro.cacciari@polymtl.ca (P.P. Cacciari), viana@fe.up.pt (A.J.P. Viana da Fonseca), hugocsf@ufrgs.br (H.C. Scheuermann Filho), alexia-wagner@hotmail.com (A.C. Wagner), carvalho.jv@ufrgs.br (João Vítor de Azambuja Carvalho), lucas@ufrgs.br (L. Festugato), consoli@ufrgs.br (N.C. Consoli).

https://doi.org/10.1016/j.sandf.2024.101438

Nomenclature

B	Skempton parameter
CSL	critical state line
ICL	isotropic compression line
D	dilation rate $= d\varepsilon_v/d\varepsilon_s$
D_{min}	maximum dilation rate (in modulus)
ϕ'	effective stress friction angle
ϕ_{cs}'	critical state friction angle
e	void ratio
e_0	void ratio prior to consolidation (molding void ratio)
e_c	void ratio after consolidation
e_{sh}	void ratio at the end of shearing
ν	specific volume $= 1 + e$
M	critical state stress ratio
M_{tc}	critical state stress ratio at triaxial compression
M_{te}	critical state stress ratio at triaxial extension
η	stress ratio $= q/p'$
η_{max}	top stress ratio $= q/p'$
P'	mean effective stress
p'_0	mean effective stress at the beginning of the shearing phase
p'_f	mean effective stress at the end of the shearing phase
q	deviatoric stress $(\sigma_1 - \sigma_3)$
σ_1, σ_3	principal stresses
u	pore water pressure
θ	Lode′s angle
IOT	iron ore tailings
CIU	isotropically consolidated undrained triaxial compression test
CID	isotropically consolidated drained triaxial compression test
CKU	K-consolidated undrained triaxial compression test
CKUE	K-consolidated undrained triaxial extension test
CKDE	K-consolidated drained triaxial extension test
PI	plasticity index
ε_a	axial strain
ε_s	shear strain
ε_v	volumetric strain
w	water content
w_L	liquid limit
λ	slope of the critical state line
Γ	intercept of the critical state line
Ψ	state parameter defined as the difference between the void ratio (e) and the critical state void ratio (e_c) at the current mean effective stress
Ψ_{Dmin}	state parameter at top dilation rate

deposited tailings, characterizing the upstream construction method (Consoli et al., 2022). Nonetheless, once the tailings are routinely found saturated and in a loose state, elevated risks associated with the operation and maintenance of such structures exist (Islam and Murakami, 2021; Viana da Fonseca et al., 2022; Yao et al., 2021; Yin et al., 2011).

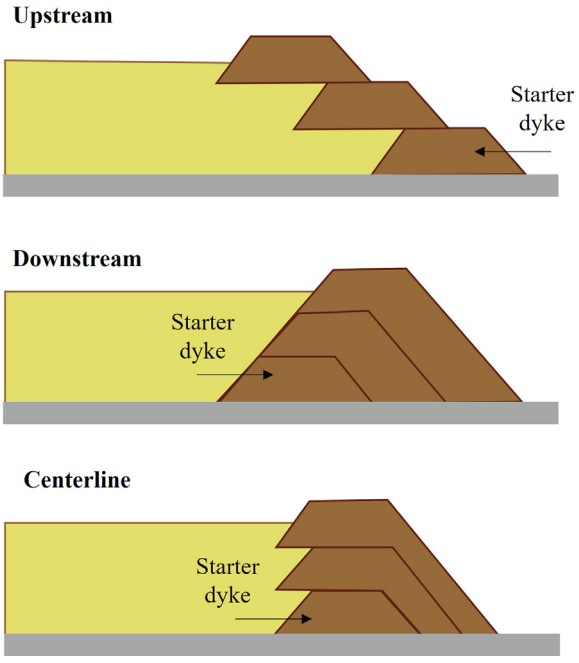

Fig. 1. Types of sequentially raised tailings dams.

Filtered tailings disposal (dry stacking) appears as an alternative to overcome a series of issues related to the traditional slurry disposal of tailings in impoundments (Gomes et al., 2016). It might be, as well, an option for usage in the de-characterization process of an existing dam. Essentially, the tailings are brought to an unsaturated condition via vacuum and/or mechanical press filtration, and they turn to present the consistency of moist sand or silty sand (Lupo and Hall, 2010). At this filtered condition, the material can be stacked and compacted in large piles. As a reason, concurrently with a reduction in land requirements for disposal, a decrement in the operational costs is also observed since the land reclamation can be carried out concomitant with the tailings′ deposition (Davies, 2011). Still, the comprehension of the compacted fills performance is essential for the design and operation of dry stacking tailings facilities.

However, studies of tailings have mainly focused on their mechanical response under loose and saturated conditions at lower pressures, mostly directed to the evaluation of liquefaction susceptibility. Such conditions are usually found in conventional tailings storage facilities, like dams. The clastic and anthropic nature of the iron ore tailings

influence their response (K-consolidation, dilatancy, extension tests, among others), considering different compaction conditions (as addressed herein) and confining pressures. These topics were not fully comprehended in previous works, particularly considering iron ore tailings. The present research directs to alternative disposition method conditions, usually found in stacking solutions. The evaluation of tailings in states other than those usually reported, focusing on their disposition in dry stacking facilities, under dense conditions and elevated pressures, is also a novelty of this research.

Accordingly, the present work assesses the mechanical response of compacted iron ore tailings through compression and extension drained (CID) and undrained triaxial (CIU and CKU) tests conducted over a wide range of effective confining pressures (p'_0 ranging from 75 to 8,000 kPa). The specified range of effective confining pressures was selected to evaluate the material behavior under stress levels potentially found in field applications. As stacking piles are expected to reach heights greater than 300 m, a broad range of effective confining pressures was adopted. The effect of the compactness was also investigated as the specimens were compacted to different initial void ratio values (e_0), being all the results evaluated in the light of Critical State Soil Mechanics. The considerations made by Jefferies (2022) on the state control of soil behavior were utilized. Complementary triaxial extension tests were also undertaken to enlarge the understanding of the material's response under non-conventional stress paths, reflecting the intricate loading conditions that mine tailings experience within these piles. In the context of possible alterations to the critical state line and susceptibility to liquefaction, evaluating the impact of particle breakage was also an aspect of the study. Through a comprehensive analysis of the obtained results, this work aims to broaden the knowledge on the mechanical response of iron ore tailings.

2. Background on Brazilian iron ore tailings storage facilities

Understanding the geotechnical properties of iron ore tailings is currently one of the major challenges in the mining industry. Tailings storage facilities (TSFs) are among the most challenging structures to operate in the mining industry, mainly due to the gradual necessity of expansion, as schematically shown in Fig. 1. The density and fineness of the tailings' particles, typically uniform with little or no plasticity, usually define the behavior of the tailings at TSF. Some of these tailings have demonstrated brittle behavior, which increases the criticality of structures close to areas occupied by humans.

Brazil's first industrial iron ore extraction occurred in Quadrilátero Ferrífero (QF). Today, the region remains among the most significant iron ore producers in a global perspective. The area known as QF is in the central region of the state of Minas Gerais in Brazil. It comprises a series of hills covering approximately 7,000 km^2. The QF deposit was formed in the lower Proterozoic between 1.9 and 2.7 billion years ago. With approximately 200 million tons of iron ore production per year, the QF is responsible for approximately 40 % of all Brazilian iron ore production. On the other hand, there is a large generation of waste from processing these ores, mainly because the QF is exploring relatively poorer reserves. In this context, the daily generation of tailings in the main industrial complexes of the QF can vary between 30 and 90 thousand tons.

After many years of mineral industry operations in the QF, the region most conducive to tailings disposal has become unavailable. Many constraints hamper the utilization of conventional TSFs in the remaining areas. There is a need to reconcile tailings, disposal, and mining activities to produce lower environmental and social impacts, highlighting the importance of understanding the geotechnical behavior of tailings. Thus, national legislation has been revised, indicating an urgent need to safely dismantle dozens of upstream tailings dams in the QF region.

In addition, recent accidents in the region, such as the failure upstream dams that occurred in Fundão, in 2015, and in Brumadinho, in 2019 (Islam et al., 2021; Lyu et al., 2019), had a great social and economic impact, significantly reducing society's receptivity to new dam projects built with tailings. In the same way, companies in the sector have been strongly pressured by civil society, the government and inspection and licensing bodies to present alternative solutions to this problem. In this context, the disposal of dry tailings in piles (Dry Stack Tailings Storage Facility - DTSF) is being adopted to contribute to the continuity of mining activities in the region by reducing the volumes of tailings destined for dams. In this approach, the moisture content of the tailings is reduced to the point where they can be compacted in stacks, resembling conventional embankments and landfills. This process involves mechanical dewatering techniques such as filtration, centrifugation, or using specialized machinery to remove excess water from the tailings. Since there are projects under study and implementation to construct DTSFs that can exceed three hundred meters, it will be feasible to deal with the high rate of tailings generation, thus reducing the impacted area because of the flexibility of this method that allows working with compacted material throughout the deposit.

It should be noted that the change in methodology will only reduce risks if it is well-grounded in a solid understanding of tailings behavior. The relevance and potential impact of some civil structures have made it evident that the design of a geotechnical work cannot be limited to current practices.

3. Experimental program

The experimental program was divided into two parts. First, the physical characteristics of the iron ore tailings were determined. Then, 26 conventional triaxial compres-

sion tests and 6 triaxial extension tests were conducted. The results were analyzed in the light of Critical State Soil Mechanics (CSSM), particularly with respect to the influence of the effective stress paths in the CSSM parameters.

3.1. Materials

The filtered iron ore tailings (IOT) were collected after a vacuum filtration process of total tailings (flotation and slimes) derived from a mine situated in the Quadrilátero Ferrífero (Iron Quadrilateral), which is located in the province of Minas Gerais, Brazil. Table 1 summarizes the main physical characteristics of the tailings. Fig. 2 exhibits the particle size distribution (PSD) of the non-sheared material and the material compacted at 100 % of compaction degree at standard effort (100 N) consolidated at 200 kPa, 900 kPa and 4,000 kPa of mean effective confining stress and sheared under drained conditions (CID). They were obtained via sieve and sedimentation analysis according to ASTM D7928 (ASTM, 2021a). The Atterberg limits and the specific gravity were evaluated, respectively, according to ASTM D4318 (ASTM, 2017a) and ASTM D854 (ASTM, 2014). The minimum (e_{min}) and maximum (e_{max}) void ratios were evaluated in agreement with ASTM D4254 (ASTM, 2016) and ASTM D4253 (ASTM, 2017b), respectively. The compaction characteristics were assessed using Proctor compactions tests on both the standard (ASTM, 2021b) and modified (ASTM, 2021c) efforts, and the results are presented in Fig. 3. The filtered IOT is classified as low plasticity silt (ML) in accordance with the Unified Soil Classification System (ASTM, 2017c). Mineralogically, the IOT was characterized by an associated analysis of scanning electron microscope with two energy dispersive spectroscopy (SEM-EDS). This equipment setup has enabled the quantification of the mineral phases. Therefore, the IOT is mainly constituted by quartz (78.4 %), iron oxide (17.2 %), feldspar (1.4 %), kaolinite (1 %), and chlorite (1 %), amongst other minor crystals. Distilled water was used throughout this research.

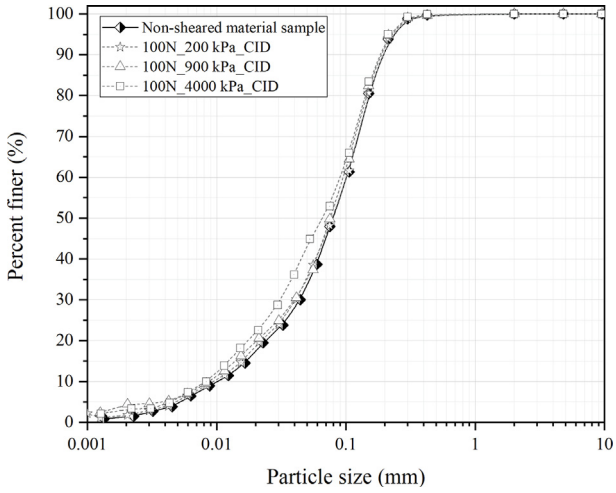

Fig. 2. Particle size distribution of the iron ore tailings.

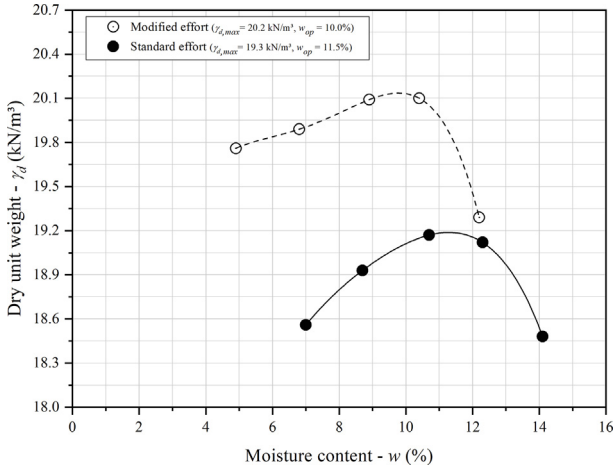

Fig. 3. Compaction characteristics of the iron ore tailings.

Table 1
Physical properties of iron ore tailings.

Parameters	Value
Specific gravity – G_s	3.064
Gravel (%)	0
Coarse sand (%)	0.0
Medium sand (%)	0.0
Fine sand (%)	37.5
Silt (%)	57.5
Clay (%)	5.0
w_L (%)	–
PI (%)	Non-plastic
ASTM-USCS Classification	ML
Maximum void ratio – e_{max}	1.284
Minimum void ratio – e_{min}	0.357
Optimum water content at Standard Effort – w_{opt} (%)	11.5
Maximum dry density at Standard Effort –γ_{dmax} (kN/m^3)	19.3
Optimum water content at Modified Effort – w_{opt} (%)	10.0
Maximum dry density at Modified Effort – γ_{dmax} (kN/m^3)	20.2

The beneficiation processes the tailings undergo provides them with characteristics distinct from conventional geomaterials. The tailings usually present characteristics highly dependent on the parent ore, marked angularities, high surface roughness, heterogeneous particle shape and fine particles, of plastic or non-plastic nature (Fourie et al., 2022; Li et al., 2018; Yang et al., 2019). Fig. 4 presents Scanning Electron Microscopy (SEM) images of the original tailings considered in this paper that highlight the observation of some of these features.

4. Methods

4.1. Specimens molding

For the triaxial compression and extension tests, cylindrical specimens (50 mm in diameter and 100 mm in height) were molded using the moist tamping method (Corrêa and Oliveira Filho, 2019; David Suits et al., 2003; Selig and Ladd, 1978). Thus, moist tailings layers were deposited inside a split mold and manually tamped to the assigned degree of compaction. Six layers were used in this process, being the top of the first, second, third, fourth and fifth layers scarified to guarantee the adherence of the subsequent layer. The latex membrane, which was going to involve the test specimen during the triaxial test, was positioned inside the split mold with the aid of a vacuum pump. This facilitated the specimen's molding and handling, particularly at the loosest conditions. Four degrees of compaction relative to the standard proctor effort (i.e., 75, 90, 97, and 100 %) and one degree of compaction with respect to the modified proctor effort (i.e., 100 %) were established. These compaction degree values were chosen to encompass a broad spectrum of compaction conditions, aiming to replicate practical levels of compaction for the dry stacking of iron ore tailings. It is important to note that in field conditions, achievable compaction degrees can vary within a certain range. The 100 % compaction degree associated with the modified Proctor effort represents the maximum achievable densification under field conditions, while the other values mimic typical compaction conditions encountered in the field. Thence, it is fundamental to understand the mechanical response over a broad range of compacities. Based on the results depicted in Fig. 3, a single moisture content (w) of 10 % was chosen irrespective of the adopted dry unit weight.

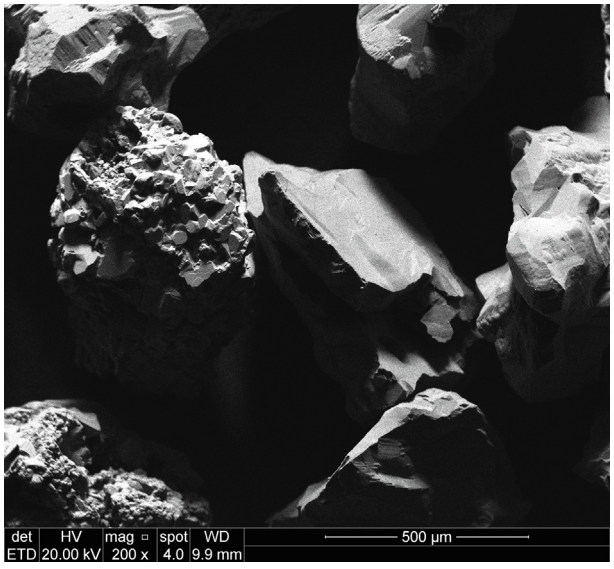

Fig. 4. SEM images of original tailings particles demonstrating surface roughness and angularity.

4.2. Triaxial compression tests

Conventional isotropically consolidated drained (CID) and isotropically consolidated undrained (CIU) triaxial tests were undertaken in order to assess the mechanical response of the iron ore tailings at a broad range of initial effective confining pressures (p'_0 = 75 kPa to p'_0 = 8,000-kPa). The specified range of effective confining pressures was selected to evaluate the material behavior under stress levels potentially found in field applications. As stacking piles are expected to reach heights greater than 300 m, a broad range of effective confining pressures was adopted. In addition, 3 K-consolidated undrained triaxial compression tests (CKU) were also carried out using a K (σ'_h/σ'_v) of 0.70 during the consolidation stage to check for possible alterations on the liquefaction susceptibility for the loosest samples. The adopted K value of 0.70 was selected based on previous studies (e.g., Fotovvat and Sadrekarimi, 2022; Fourie and Tshabalala, 2005). Table 2 summarizes the data relative to the 26 triaxial tests. The following notation was used to identify each test: CE_FkPa$_G$, where C is the degree of compaction (75 %, 90 %, 97 % or 100 %), E is the respective compaction effort (N = standard proctor or M = modified proctor), F is the initial confining pressure (75, 100, 150, 200, 300, 400, 800, 900, 1600, 4000, 6000 or 8000 kPa) and G is the test type (CID, CIU or CKU). It is worth mentioning that the molding void ratio (e_0), the after-consolidation void ratio (e_c), and the after-shearing void ratio (e_{sh}) are depicted for each tested specimen.

The recommendations stated by ASTM D7181 (ASTM, 2020a) and ASTM D4767 (ASTM, 2020b) were followed. Thus, all the tests were performed on fully saturated specimens that have been submitted to a saturation process composed of carbon dioxide percolation, water percolation and application of back-pressure increments (maintaining the mean effective stress constant and equal to 15 kPa). The Skempton B values obtained once the saturation was finished are displayed in Table 2, and most of them were greater than 0.98. In addition, P-wave velocity (V_p) was measured by means of bender elements installed at the top and bottom caps in all triaxial specimens after the saturation process was finished. All tested specimens presented V_p nearer or higher than 1500 m/s, value that is associated with the specimen's full saturation (Viana da Fonseca et al., 2021). The consolidation phase was con-

Table 2
Summary of triaxial compression tests data.

Test	Shearing	B	p_0' (kPa)	p_f' (kPa)	q_f (kPa)	q_f/p_f'	e_0	e_c	e_{sh}
100M_100	CID	0.98	100	215	340	1.58	0.49	0.48	0.55
100M_200	CID	0.99	200	409	625	1.53	0.50	0.48	0.55
100N_75	CID	0.99	75	162	260	1.60	0.56	0.54	0.59
100N_100	CID	0.98	100	200	302	1.51	0.56	0.53	0.61
100N_150	CID	0.98	150	308	472	1.53	0.54	0.53	0.58
100N_200	CID	0.94	200	398	593	1.49	0.55	0.51	0.56
100N_900	CID	0.98	900	1774	2618	1.47	0.55	0.51	0.55
100N_4000	CIU	0.94	4000	7002	9044	1.31	0.55	0.48	0.46
100N_6000	CIU	1.00	6000	6268	8413	1.34	0.55	0.49	0.49
97N_400	CIU	0.99	400	1135	1598	1.40	0.60	0.58	0.58
97N_800	CIU	0.98	800	1541	2065	1.37	0.60	0.58	0.58
97N_1600	CIU	0.98	1600	2190	3039	1.39	0.59	0.55	0.55
90N_100	CID	1.00	100	186	256	1.38	0.69	0.68	0.68
90N_300	CID	0.99	300	564	789	1.40	0.69	0.66	0.65
90N_8000	CIU	1.00	8000	2759	3605	1.31	0.69	0.55	0.55
75N_200	CID	0.97	200	379	538	1.42	1.08	0.75	0.65
75N_400	CID	0.99	400	758	1076	1.42	1.08	0.73	0.62
75N_800	CID	0.99	800	1507	2121	1.41	1.07	0.70	0.59
75N_1600	CID	0.97	1600	2999	4194	1.40	1.04	0.65	0.54
75N_200	CIU	1.00	200	1	6	0	1.08	0.75	0.75
75N_400	CIU	0.98	400	10	17	1.70	1.07	0.73	0.73
75N_800	CIU	1.00	800	44	67	1.51	1.07	0.69	0.69
75N_1600	CIU	0.99	1600	507	702	1.39	1.04	0.64	0.64
75N_300	CKU[a]	0.99	300	5	17	3.40	1.07	0.73	0.73
75N_600	CKU[a]	1.00	600	43	59	1.37	1.07	0.70	0.70
75N_1200	CKU[a]	1.00	1200	160	223	1.39	1.07	0.65	0.65

[a] K-consolidated undrained triaxial compression

ducted by the increment in the chamber pressure at a constant rate of 50 kPa per hour up to the desired σ'_3 value. Such rate was adequate as no excess pore pressure was generated during this procedure. Once the consolidation was terminated, the shearing started at a rate of 1.50 mm per hour which was adequate to guarantee the proper drainage during the CID tests. For the CID tests, the volume change was evaluated by measuring the flow volume of water entering/leaving the specimen with an automated volume gauge. Still, the after-shearing void ratio was determined by the end-of-test soil freezing technique for both the CIU and CID tests (Sladen and Handford, 1987, Viana da Fonseca et al., 2021). The confinement pressure and back-pressure were controlled by two computer-assigned digital pressure/volume controllers.

4.3. Triaxial extension tests

K-consolidated undrained triaxial extension tests (CKUE) and K-consolidated drained triaxial extension tests (CKDE) were also carried out for a few specimens. The intention was to further characterize the mechanical response of the iron ore tailings, particularly with respect to the impact of different effective stress paths on the critical state. K-consolidation has been previously employed in tailings, and as-like materials to simulate eventual departures of the isotropic state of stress of the material after sedimentation (Fotovvat and Sadrekarimi, 2022; Fourie and Tshabalala, 2005).

The same equipment setup for the triaxial compression tests was used for the extension tests. The main difference is that a suction cap was adopted in order to enable the vertical unloading of the specimen. In this regard, Table 3 displays the main data relative to the 6 extension tests which were performed on specimens molded at 97 % of the energy relative to the standard Proctor effort (97 N). The saturation process was identical to what was described for the compression tests, and the consolidation was carried out using a K of 0.70. The extension phase was strain-controlled, being the axial stress (σ'_a) relieved at a rate of 1.50 mm per hour while the horizontal stress (σ'_h) was kept constant. After the test was finished, the end-of-test soil freezing technique was, as well, applied to estimate the e_{sh}.

5. Results and discussion

5.1. General aspects

The stress–strain response of the iron ore tailings (IOT) under drained conditions is presented in Fig. 5a (dense specimens) and Fig. 5b (loose specimens). Due to the wide range of employed confining pressures, the deviatoric stress (q) was normalized by the initial mean effective stress (p'_0). The two loosest specimens (75 N and 90 N) have shown a ductile response accompanied by a fully contractive behavior. An exception was test 90N_100kPa_CID which slightly dilated after compression at the start of the shearing. On

Table 3
Summary of triaxial extension tests data.

Test	Shearing	B	p_0' (kPa)	p_f' (kPa)	q_f (kPa)	q_f/p_f'	e_0	e_c	e_{sh}
97N_300	CKDE	0.98	300	201	−187	−0.93	0.61	0.56	0.56
97N_600	CKDE	0.98	600	389	−408	−1.05	0.61	0.55	0.55
97N_1200	CKDE	1.00	1200	790	−780	−0.99	0.60	0.55	0.54
97N_300	CKUE	0.99	300	390	−394	−1.01	0.61	0.57	0.57
97N_600	CKUE	1.00	600	542	−539	−0.99	0.61	0.54	0.54
97N_1200	CKUE	1.00	1200	708	−674	−0.95	0.61	0.55	0.55

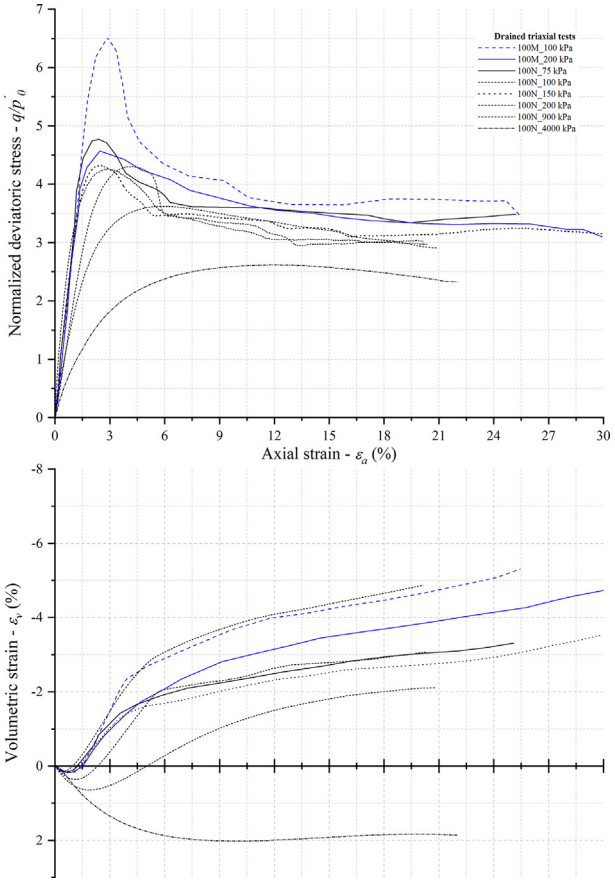

Fig. 5. CID triaxial tests (a) dense specimens (b) loose specimens.

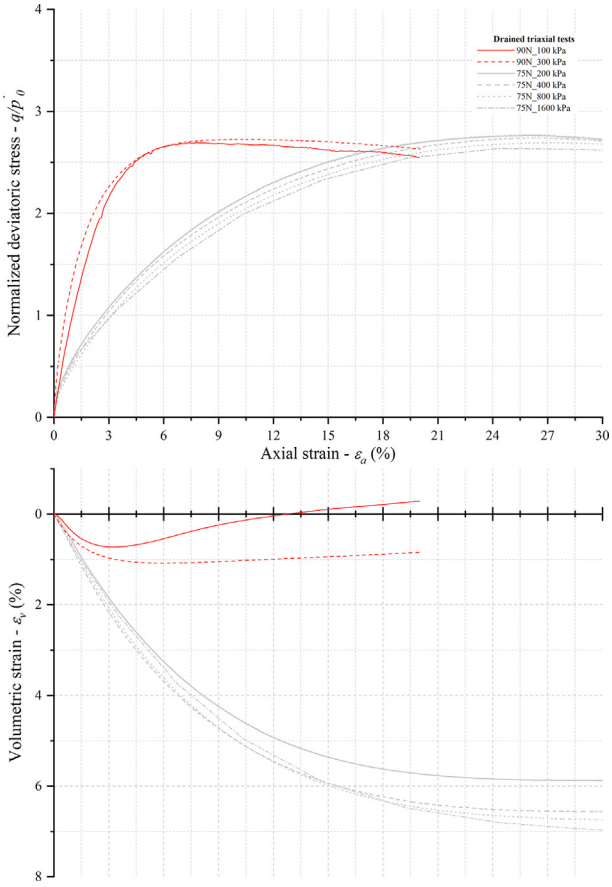

Fig 5. *(continued)*

the contrary, all but one of the specimens molded at the two highest compaction degrees (100 M and 100 N) have presented a peak strength associated with an initial contractive response which was followed by a remarkably dilatant trend. The exception was the 100N_4000kPa_CID test which has only contracted owing to the elevated confinement level. Such behavior is analogous to the observed for soils, where the confinement restrains and even inhibits dilation. Fig. 5 also indicates that looser specimens tend to have stability in volumetric strains at lower levels of axial strains. In contrast, denser specimens had not reached such a steady state and were still dilating when the shearing was terminated. These patterns evidence that some specimens have not reached the critical state during the triaxial tests.

Regarding the undrained tests shown in Fig. 6a (isotropic consolidation) and Fig. 6b (K-consolidation), a substantial loss of strength due to positive pore pressure generation has taken place amongst the least dense specimens (75 N and 90 N) for both consolidation stress paths. This was accompanied by a strain-softening response and is indicative of susceptibility to static liquefaction, particularly for the loosest specimens sheared at low confinement levels. The denser samples (97 N and 100 N) showed an initial positive pore pressure variation which then turned into a negative pore pressure change that was accompanied by a strain-hardening stress–strain response.

The normalized stress (q/p') versus ε_a results are exhibited in Fig. 7a for the CID tests and in Fig. 7b for the CIU tests. Fig. 7b further compares the results of the three K-consolidated tests which attests the similarity between the K-consolidated samples and the isotropic consolidated ones. Both presented a major loss of strength at lower con-

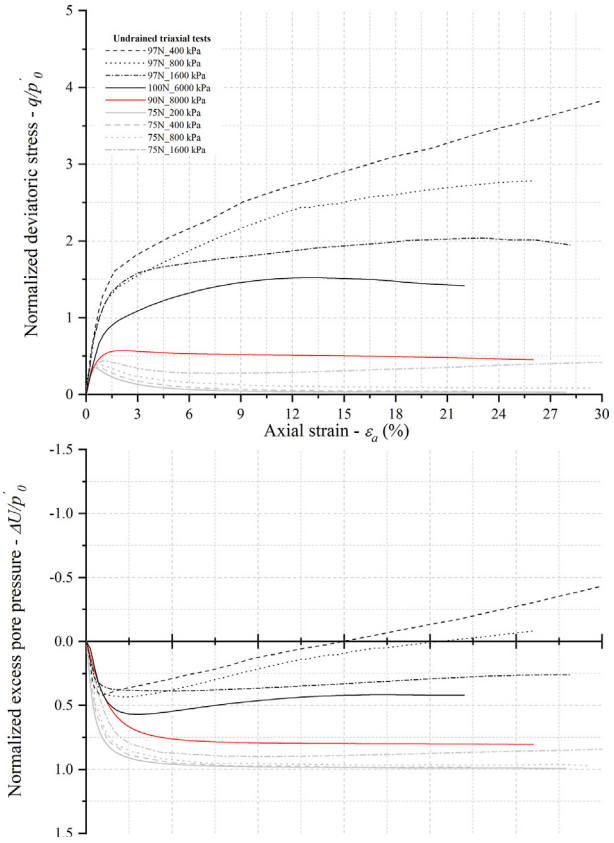

Fig. 6. Undrained triaxial tests (a) isotropic consolidation (b) *K*-consolidation.

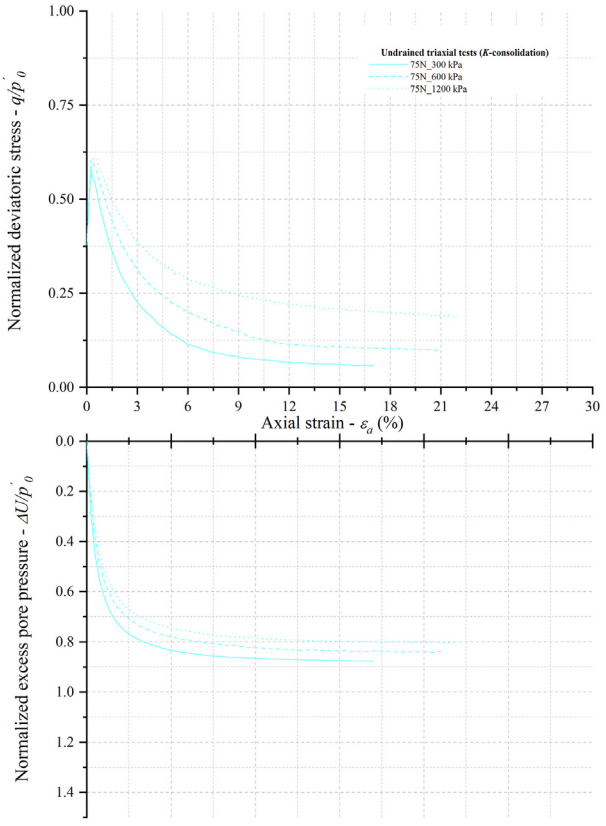

Fig 6. *(continued)*

fining pressures. Therefore, the effect of K-consolidation was restricted to the consolidation phase where the specimens experimented larger strains due to the conjunction of compression and shear efforts. Then, the different compression paths (similar to those occurring in the field) do not seem to have any influence on the shear behavior of the material at large strains. The normalized results reveal that most tests converge to a stress ratio (η) value of around 1.40. Such η value was obtained from the response of loose specimens (75 N compaction degree) because of marked strain localization occurring in dense specimens. Also, the majority of the densest samples had not yet reached such η value as they were still presenting volumetric/pore pressure variations at the end of the shearing, thus have not yet reached a critical state condition. In addition, the 75N_200kPa_CIU, the 75N_400kPa_CIU, and the 75N_300kPa_CKU tests presented unrealistic final q/p' values due to the substantial loss of strength associated with the excessive generation of pore water pressure.

The outcomes relative to the extension tests are depicted in Fig. 8a (drained tests) and Fig. 8b (undrained tests) and indicate, after an initial compression, a dilatative trend for the drained tests which is reflected by a tendency of diminishing pore pressure amongst the undrained tests. A strain-hardening behavior is noticed on the normalized stress–strain plot, and no tendency to static liquefaction was

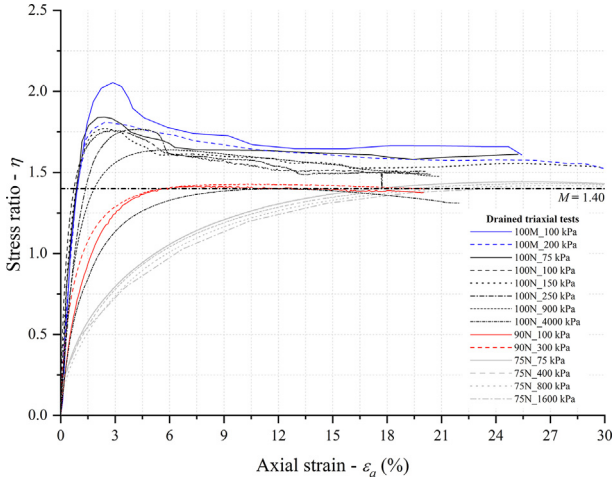

Fig. 7. Normalized stress–strain response (a) CID tests (b) CIU and CKU tests.

found. This strain-hardening trend was more in evidence for the lower confining pressure levels and under undrained condition. Then, the results show that compacting the tailings provided a dense condition that can avoid the occurrence of static liquefaction, regardless of the stress path (compression or extension) to which the material is subjected in the field. Yet, due to equipment limitations, higher values of axial deformation have not been reached: the critical state has not been necessarily achieved for these tests.

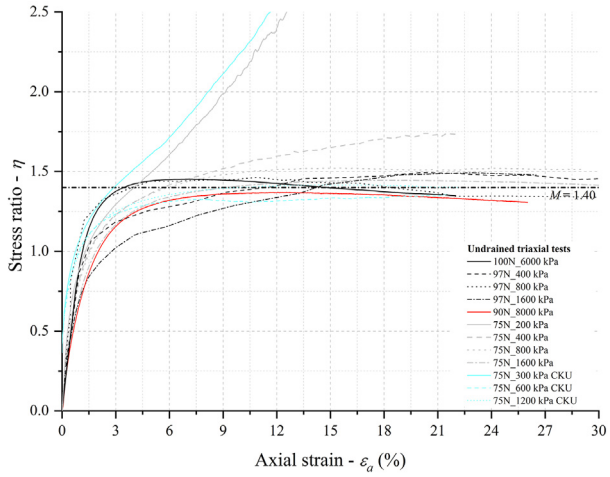

Fig 7. *(continued)*

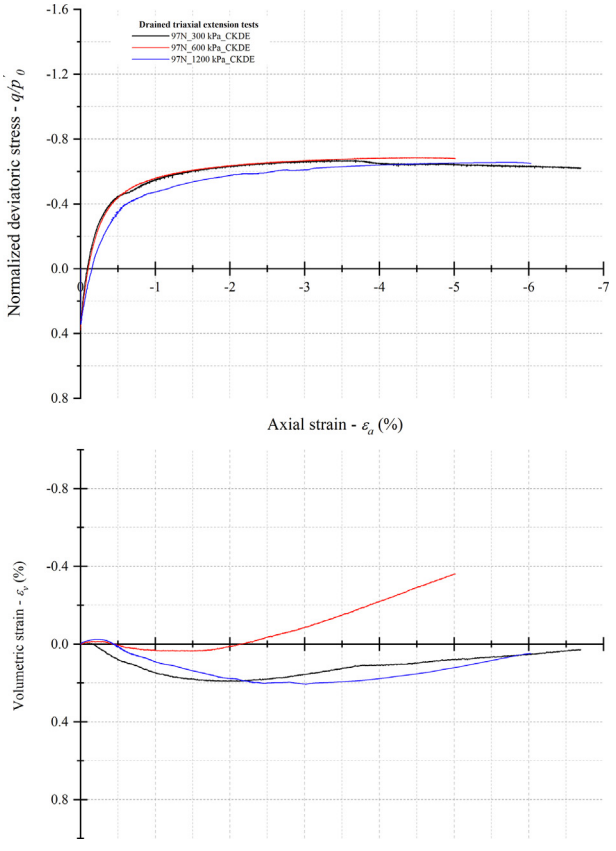

Fig. 8. Triaxial extension test results (a) drained tests (b) undrained tests.

It is not possible to directly compare the compression and extension tests results because of the influence of the intermediate stress on response. Thus, a normalization accounting for the effect of Lode's angle (θ) was considered (Poorooshasb, 1989), in which the stress ratio is scaled by a function $g(\theta)$. The formulation adopted for the scaling function $g(\theta)$ followed Jefferies and Shuttle (2002), as presented in Eq. (1).

$$g(\theta) = M_\theta / M_{tc} \tag{1}$$

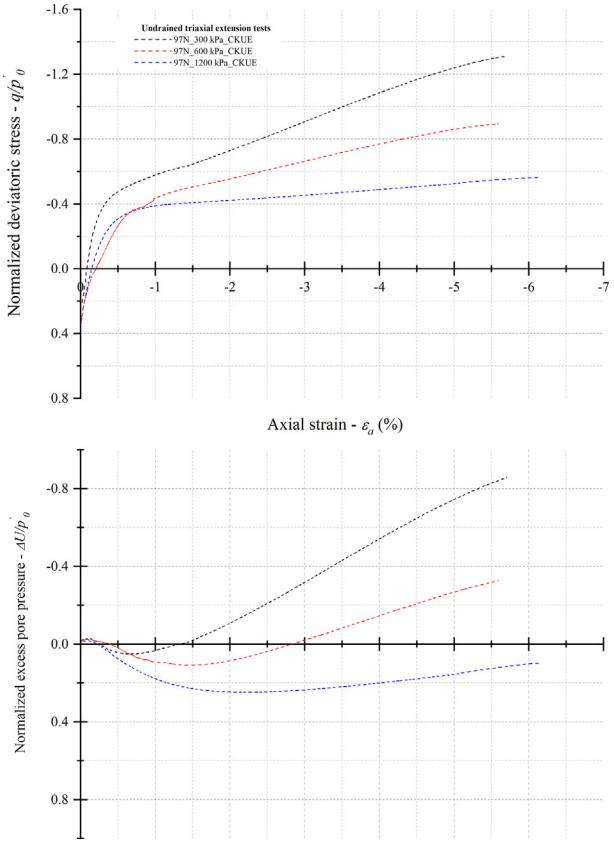

Fig 8. *(continued)*

where M_θ is the slope of the critical state stress ratio as a function of θ, and M_{tc} is the critical state stress ratio for triaxial compression.

This normalization can account for the effect of mean effective stress and intermediate stress, allowing to compare the behavior of extension and compression tests. Also, the pore pressure was further normalized with respect to initial confining stress (p'_0). By comparing the compression and extension tests with similar void ratio after consolidation (Fig. 9), it can be seen that the specimens subjected to extension stress paths presented higher negative pore pressure generation than those under compression paths, which is associated with the influence of the intermediate stress (Perić and Ayari, 2002). Moreover, the normalized stress ratio results demonstrated the tendency to convergence to unique $q/[p'g(\theta)]$ value with further strains. This approach could be used in analyzing other stress paths (such as plane strain conditions) and helping to investigate the influence of intermediate stress on the behavior of tailings.

5.2. Stress paths and critical states

Fig. 10 presents the normalized stress paths of all tests conducted. The normalization by confining stress was adopted to allow the representation of tests over the broad range of pressures tested more easily. Within this normal-

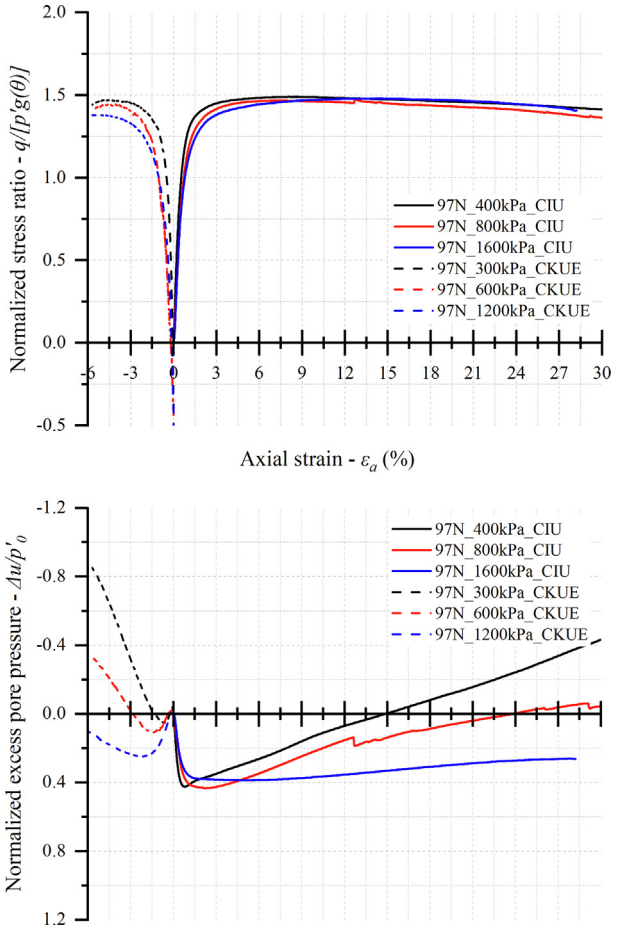

Fig. 9. Normalized stress ratio response of compression and extension tests.

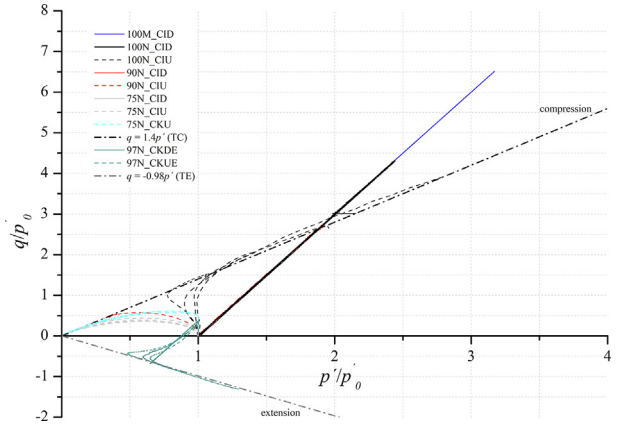

Fig. 10. Stress paths.

ization, all compression drained stress paths get overlapped. However, the undrained stress paths preserve characteristics of behavior that can be observed. The strain-hardening behavior for dense samples under undrained compression and extension tests can also be clearly observed by the stress paths in Fig. 10, supporting that liquefaction did not occur for these cases.

The critical state is characterized by the absence of volume, deviatoric stress, and mean normal effective stress variations during the shearing of a soil mass and is generally attained at large deformation values (Been et al., 1991; Kuhn, 2016; Wood, 2008). From previously presented discussions, it is presumable that most of the compression samples had reached (loosest specimens) or were not far from reaching (densest specimens) this condition when the shearing was terminated. In this regard, the slope of the presumed critical state lines in the p'- q/p'_0 plane has resulted in a critical state stress ratio (M_{tc}) value of 1.40. This corresponds to a critical state friction angle (ϕ_{cs}') of 34.6°. The final test data were used in this critical state analysis. Considering the endpoints of the extension tests, a M_{te} value of 0.98 was obtained, corresponding to a ϕ_{cs}' equal to 35.8°. These results are shown in the stress paths displayed in Fig. 10. The different M values obtained for extension and compression tests are a function of the proportion of intermediate principal stress (represented by Lode's angle - θ). The more severe loading condition (extension, where the intermediate principal stress is equal to the major principal stress) results in lower strength (lower M). However, the variation of M does not imply that the critical state friction angle varies, confirming the slight difference observed here.

In order to determine the critical state line (CSL) of the iron ore tailings in the specific volume v: log p' plane, the points relative to the final specific volume (v) were plotted as a function of the corresponding mean effective stress values at the end of the test (p_f'). These outcomes are depicted in Fig. 11. In this sense, two attempts were made to fit the CSL disregarding the data relative to the densest samples (i.e., 100 N and 100 M) as they have not reached the critical state. The first attempt refers to a conventional semi-log idealization curve of the CSL covering the range from 200 to 8,000 kPa. This possesses the form of (Eq. (2). The results concerning the loosest samples sheared at undrained conditions under the three lowest initial confining pressures (i.e., σ'_3 = 200, 400 and 800 kPa) were

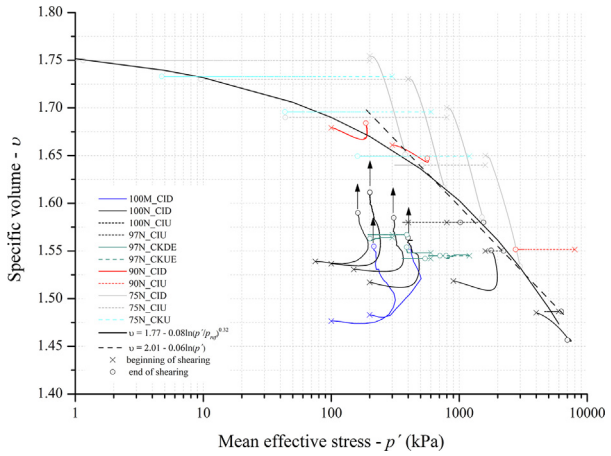

Fig. 11. Critical state line in the υ – log p' plane.

neglected from this analysis owing to the substantial loss of strength registered during the shearing. For (Eq. (2), the slope (λ) of the critical state line (CSL) was equal to 0.06, and the intercept (Γ) was 2.01.

$$\upsilon = \Gamma - \lambda \ln p\hat{A}' \tag{2}$$

A second attempt fits all endpoints (excluding densest samples), throughout the stress range, with a power law (e.g., Jefferies and Been, 2016). This adjustment is a higher-order idealization that captures CSL curvature as expressed by relationship (Eq. (3). In this case, the slope (b) of the critical state line (CSL) was equal to 0.08, the intercept (a) was 1.77, the exponent (c) was 0.32 and the p_{ref} used was 100 kPa.

$$\upsilon = \mathrm{a} - b\left(\frac{p\hat{A}'}{p_{ref}}\right)^{c} \tag{3}$$

Considering the range of the studied stresses, the specimens molded at different ν values converged, or were converging, towards a unique CSL in the ν: log p' plane. Moreover, the proposed curved CSL was able to capture the endpoints data over a wider range of stresses than the semi-log idealization. The first was initially flatter up to a p' of around 150 kPa, then becoming more inclined with a slope similar to the latter.

Qualitatively, similar CSLs curved shapes were reported by Bedin et al. (2012) and by Li et al. (2018) for gold tailings, by Carrera et al. (2011) for fine sand and silt and, partially, by Li and Coop (2019) for Middle Beach (MB) and Upper Beach (UB) iron ore tailings. Li and Coop (2019) have also reported a linear CSL considering the same material but gathered from the pond (PO). All those results are summarized in Fig. 12, in which curved shape CSLs were fitted for all the test results reported by those authors but the pond iron ore tailings. As well, the main characteristics relative to the particle size distribution of those tailings are summarized in Table 4. It is noticeable that the particle size distribution exerts a substantial influence with relation to the locus of the CSL as differences in the a, b, and c parameters were reported for tailings derived from the same parental material but presenting different grain size distributions.

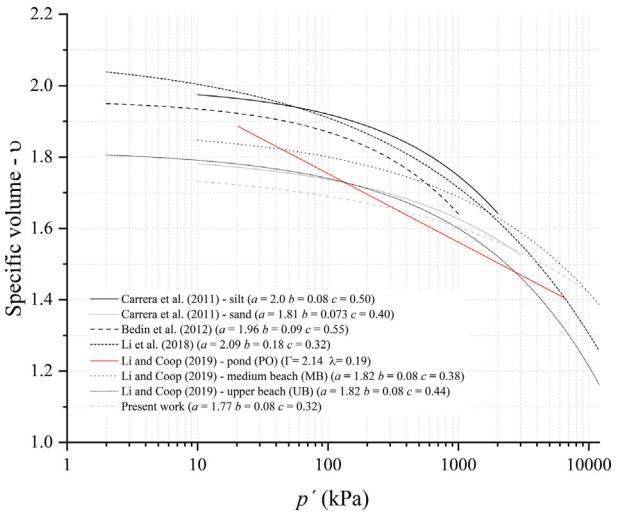

Fig. 12. Critical state lines from other works in the υ – log p' plane.

5.3. Dilatancy analysis

A stress-dilatancy analysis was performed by plotting the stress ratio ($\eta = q/p'$) as a function of the dilation rate ($D = d\varepsilon_v/d\varepsilon_s$) for the CID triaxial tests. These results are depicted in Fig. 13a and resemble the form of a typical purely frictional material. That is, the peak strengths are completely associated with dilation (Esposito and Andrus, 2017; Jefferies, 2022; Vaid and Sasitharan, 1992), and the $\eta \times D$ trends are directed towards the same critical state stress ratio value ($M_{tc} = 1.40$) as the shearing progresses. Although the densest samples have not reached the critical state, the dilation rate was decaying at the later stages of the shearing, and the tendency was pointing towards this unique M value. Considering the volume change response, all the specimens have presented an initially contractive behavior that persisted throughout the whole shearing for the initially loosest specimens (75 N). In contrast, most of the other samples have dilated after this initial compression, being the top stress ratio ($\eta_{\max}$) proportional to the modulus of maximum dilatancy (D_{min}) as shown in Fig. 13b. In other words, higher η values were attained for specimens that, besides the purely frictional strength parcel, have dilated the most. Naturally, this has occurred for the densest samples sheared at the lowest levels of confining pressures (e.g., 100M_100 kPa).

A complementary analysis was conducted via two different relationships: the state parameter (Ψ) related to the dilation rate (Fig. 14a) and the maximum dilation rate (D_{min}) correlated to the corresponding state parameter (Fig. 14b). In this regard, initially positive Ψ values denote a fully contractive behavior, whereas initially negative Ψ values indicate that dilation must take place if the critical state is to be reached at some point (Been et al., 1991). The results shown in Fig. 13a agree with the previous stress-dilatancy analysis. In brief, the dilatancy response of the loosest specimens (75 N and 90 N) had not been affected by the stress level, as shown by the superimposition of the state trends in the Ψ-D_{min} plane. Considering the densest samples (100 N and 100 M), the dilatancy paths differed for distinct mean stress levels. As well, the proportionality between Ψ at maximum dilatancy and D_{min} (Fig. 14b) suggests that higher levels of dilation must occur at specimens that are further from the critical state. Otherwise, those specimens will not reach such a state (Cuccovillo and Coop, 1999).

Jefferies (2022) proposed a formal derivation for Ψ, based on a kinematic framework for dilatancy. In his approach, the state of a sample fundamentally governs the magnitude of dilatancy rate, which in turn defines the strength mobilized. Therefore, Eq. (4) represents the rela-

Table 4
Summary of tailings data.

	Present work	Carrera et al. (2011) - sand	Carrera et al. (2011) - silt	Bedin et al. (2012)	Li et al. (2018)	Li and Coop (2019) - PO	Li and Coop (2019) - MB	Li and Coop (2019) - UB
Material	Iron ore tailings	Stava tailings		Gold tailings	Gold Tailings	Iron ore tailings		
Specific gravity	3.064	2.721	2.828	2.89–3.20	2.89	3.112	3.137	3.365
Coarse Sand (2.00 mm < d < 4.75 mm) (%)	0.0	0.0	0.0	0.0	0.0	0.0	0.0	0.0
Medium Sand (0.425 mm < d < 2.00 mm) (%)	0.0	3.3	0.0	0.0	0.0	0	0.0	16.0
Fine Sand (0.075 mm < d < 0.425 mm) (%)	37.5	96.7	15	29.0	5.0	6.0	32.0	66.0
Silt (0.002 < d < 0.075 mm) (%)	57.5	0.0	78	63.0	85.0	91	54.0	18.0
Clay (d < 0.002 mm) (%)	5.0	0.0	7.0	8.0	10.0	3.0	4.0	0.0

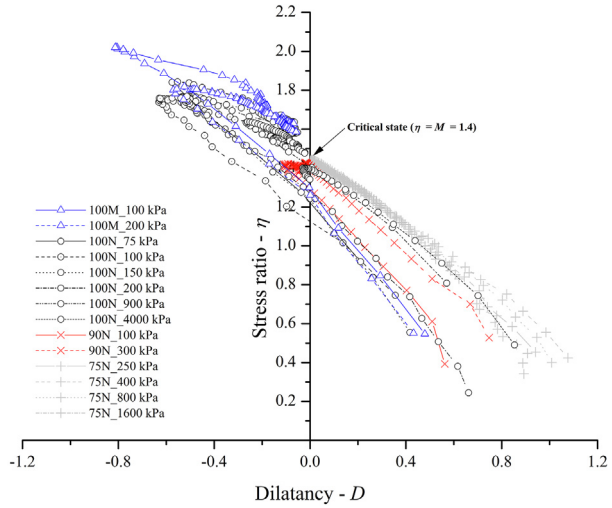

Fig. 13. Stress-dilatancy analysis (a) η versus D (b) η_{max} versus D_{min}.

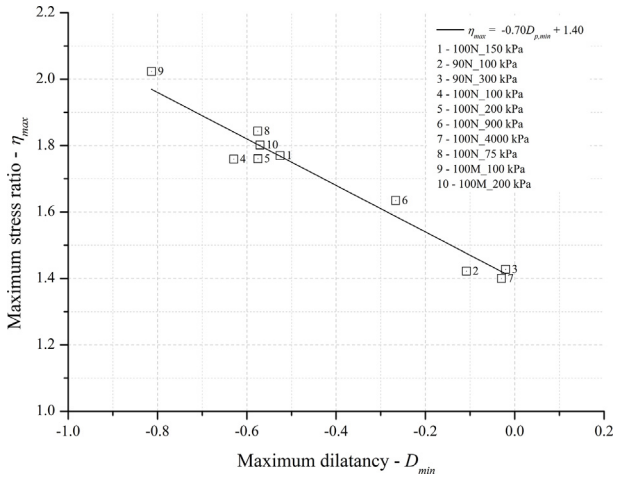

Fig 13. *(continued)*

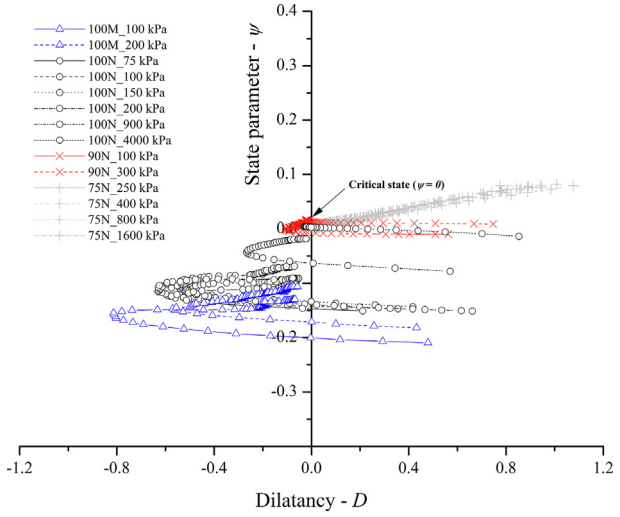

Fig. 14. State parameter-dilatancy analysis (a) Ψ versus D (b) Ψ at D_{min} versus D_{min} (c) η_{max} versus Ψ at D_{min}.

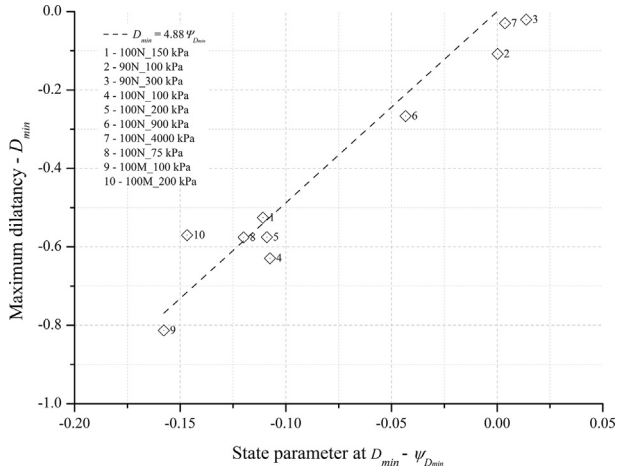

Fig 14. *(continued)*

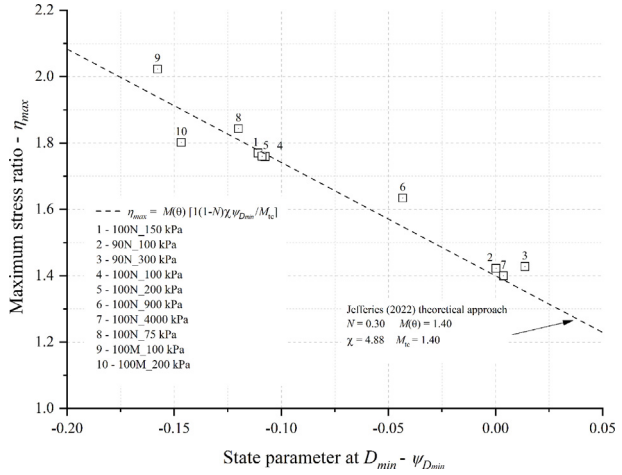

Fig 14. *(continued)*

tionship between the maximum stress ratio (η_{max}) and the state parameter at the maximum dilation rate (Ψ_{Dmin}). Following Jefferies (2022), the relationships represented in Fig. 13b and in Fig. 14b have resulted in a critical state stress ratio (M_{tc}) equal to 1.40, in a Nova's volumetric coupling coefficient (N) of 0.30, and on a scaling factor for soil dilatancy (χ)of 4.88. Such values are in the range reported by Jefferies (2022) for sandy soils and silty soils.

$$\eta_{max} = M(\theta)[1 - \frac{(1-N)\chi\psi_{D_{min}}}{M_{tc}}] \quad (4)$$

where $M(\theta)$ is the critical state stress ratio as a function of the Lode angle ($\theta = \pi/6$ for triaxial compression). Relationship (3) is graphically presented in Fig. 14c altogether with the experimental data considering the specimens which have exhibited a dilatant behavior. Promptly, a great concordance is perceived between the Jefferies (2022) theoretical approach and the attained triaxial test results. This indicates that such a relationship is adequate to model the strength-dilatancy response of the studied iron ore tailings. Besides, Fig. 14c and relationship (3) demonstrate that the greatest η_{max} values are observed on the specimens which are further from the critical state line at the peak stress, in other words, on samples that dilate the most. Thus, the good correlation between the theoretical approach and the experimental data reinforces the dependence of dilatancy on the sample's state as proposed by Jefferies (2022).

5.4. Particle breakage analysis

The particle size distribution of after-test specimens (drained tests under confining pressures of 200, 900, and 4000 kPa) was assessed through sieve and sedimentation analysis (ASTM, 2021a). Fig. 2 depicts the results obtained. Considering the PSDs obtained for the pressure range tested, it can be noticed that the degree of breakage has slightly increased with rising confining pressure. Although the differences in PSD are small, they can be associated with the occurrence of particle breakage in the form of a reduction in surface roughness, breakage of asperities, and reduction in particle angularity. The industrial nature of tailings provides them with morphological characteristics distinct from conventional materials. Therefore, for these materials, the relevance of particle breakage may be significant from lower pressures than for other conventional geomaterials.

6. Concluding remarks

Present research assessed the mechanical response of compacted iron ore tailings via drained and undrained triaxial compression and extension tests focusing on their disposition in dry stacking facilities. Therefore, the material was tested under loose and dense conditions over various confining pressures to simulate multiple boundary conditions encountered in dry stacking facilities. This encompasses the main novelty of the present study, particularly when considering the clastic and anthropic nature of the iron ore tailings. Thus, considering the boundaries of the study, the following conclusions can be drawn:

- Regardless of the K value used in the consolidation phase, the initial loosest specimens have shown a high susceptibility to static liquefaction when sheared under low levels of confinement. This indicates that the adoption of such compacity is not indicated for the dry stacking of iron ore tailings, particularly at shallow depths;
- The densest samples have not presented any susceptibility to static liquefaction as the majority of them exhibited a dilatative trend when sheared, even at higher mean stress levels;
- Even though the densest specimens have not reached the critical state, a unique curved critical state line appears to exist for the iron ore tailings. That is, these dense specimens were directing towards the fitted line when the shearing was terminated. However, it must be said that further research is still needed to clarify this point.

- The top stress ratio (η_{max}) was proportional to the maximum dilatancy (D_{min}), indicating that the peak strength is associated with a dilatant trend of the material. This is typical of a purely frictional material. Moreover, higher state parameter values, in modulus, were reported for the specimens that dilated the most, indicating that a higher dilation rate is needed if the critical state is to be reached at some point.
- The results presented herein have indicated the feasibility of dry stacking for the iron ore tailings as no abnormal response was observed throughout the triaxial tests, even in high confining pressures, which highlights the importance and the novelty of the present manuscript;
- The small degree of particle breakage identified after shearing for the stress range studied herein did not demonstrate a strong influence on the measured behavior;
- A substantial lower critical state stress ratio (M) was observed on the specimens tested for triaxial extension due to the more severe load condition this stress path imposes. However, the critical state friction angle (ϕ_{cs}') obtained was similar for extension and compression triaxial stress paths, with the value for the extension path being slightly higher (35.8° for triaxial extension and 34.6° for triaxial compression).

Acknowledgements

The authors wish to express their appreciation to VALE S.A. and Brazilian Research Council (CNPq) for their support to the research group. Special thanks are also due to Michael Jefferies (Geotechnical Senior Consultant) for several comments concerning the draft paper.

References

ASTM, 2014. Test methods for specific gravity of soil solids by water pycnometer - *ASTM D854*. ASTM International. https://doi.org/10.1520/D0854-14.

ASTM, 2016. Test methods for minimum index density and unit weight of soils and calculation of relative density - *ASTM D4254*. ASTM International. https://doi.org/10.1520/D4254-16.

ASTM, 2017a. Test methods for liquid limit, plastic limit, and plasticity index of soils - *ASTM D4318*. ASTM International. https://doi.org/10.1520/D4318-17E01.

ASTM, 2017b. Test methods for maximum index density and unit weight of soils using a vibratory table - *ASTM D4253*. ASTM International. https://doi.org/10.1520/D4253-16E01.

ASTM, 2017c. Practice for classification of soils for engineering purposes (Unified Soil Classification System) - *ASTM D2487*. ASTM International. https://doi.org/10.1520/D2487-17E01.

ASTM, 2020a. Test method for consolidated drained triaxial compression test for soils - *ASTM D7181*. ASTM International. https://doi.org/10.1520/D7181-20.

ASTM, 2020b. Test method for consolidated undrained triaxial compression test for cohesive soils - *ASTM D4767*. ASTM International. https://doi.org/10.1520/D4767-11R20.

ASTM, 2021a. Test method for particle-size distribution (gradation) of fine-grained soils using the sedimentation (hydrometer) analysis - *ASTM D7928*. ASTM International. https://doi.org/10.1520/D7928-21E01.

ASTM, 2021b. Test methods for laboratory compaction characteristics of soil using standard effort (12,400 ft-lbf/ft^3 (600 kN-m/m^3)) - *ASTM D698*. ASTM International. https://doi.org/10.1520/D0698-12R21.

ASTM, 2021c. Test methods for laboratory compaction characteristics of soil using modified effort (56,000 ft-lbf/ft^3 (2,700 kN-m/m^3)) - *ASTM D1557*. ASTM International. https://doi.org/10.1520/D1557-12R21.

Bedin, J., Schnaid, F., Da Fonseca, A.V., Costa Filho, L.D.M., 2012. Gold tailings liquefaction under critical state soil mechanics. Géotechnique 62, 263–267. https://doi.org/10.1680/geot.10.P.037.

Been, K., Jefferies, M.G., Hachey, J., 1991. The critical state of sands. Géotechnique 41, 365–381. https://doi.org/10.1680/geot.1991.41.3.365.

Carrera, A., Coop, M., Lancellotta, R., 2011. Influence of grading on the mechanical behaviour of Stava tailings. Géotechnique 61, 935–946. https://doi.org/10.1680/geot.9.P.009.

Consoli, N.C., Vogt, J.C., Silva, J.P.S., Chaves, H.M., Scheuermann Filho, H.C., Moreira, E.B., Lotero, A., 2022. Behaviour of compacted filtered iron ore tailings–Portland cement blends: new Brazilian trend for tailings disposal by stacking. Appl. Sci. 12, 836. https://doi.org/10.3390/app12020836.

Corrêa, M.M., Oliveira Filho, W.L., 2019. Impact of methods used to reconstitute tailings specimens on the liquefaction potential assessment of tailings dams. REM Int. Eng. J. 72, 507–513. https://doi.org/10.1590/0370-44672018720164.

Cuccovillo, T., Coop, M.R., 1999. On the mechanics of structured sands. Géotechnique 49, 741–760. https://doi.org/10.1680/geot.1999.49.6.741.

David Suits, L., Sheahan, T., Frost, J., Park, J.-Y., 2003. A critical assessment of the moist tamping technique. Geotech. Test. J. 26, 9850. https://doi.org/10.1520/GTJ11108J.

Davies, M., 2011. Filtered dry stacked tailings: The fundamentals. In: Tailings and Mine Waste Conference (2011: Vancouver, B.C.); University of British Columbia. Norman B. Keevil Institute of Mining Engineering. https://doi.org/10.14288/1.0107683.

Esposito, M.P., Andrus, R.D., 2017. Peak shear strength and dilatancy of a Pleistocene age sand. J. Geotech. Geoenviron. Eng. 143, 04016079. https://doi.org/10.1061/(ASCE)GT.1943-5606.0001582.

Fotovvat, A., Sadrekarimi, A., 2022. Instability of a gold mine tailings subjected to different stress paths. J. Geotech. Geoenviron. Eng. 148. https://doi.org/10.1061/(ASCE)GT.1943-5606.0002780 04022020.

Fourie, A., Verdugo, R., Bjelkevik, A., Torres-Cruz, L.A., Znidarcic, D., 2022. Geotechnics of mine tailings: A 2022 state of the art. In: Proceedings of the 20th ICSMGE-State of the art report. Rahman and Jaksa Editors, Sydney, Australia.

Fourie, A.B., Tshabalala, L., 2005. Initiation of static liquefaction and the role of K_0 consolidation. Can. Geotech. J. 42, 892–906. https://doi.org/10.1139/t05-026.

Gomes, R.B., De Tomi, G., Assis, P.S., 2016. Iron ore tailings dry stacking in Pau Branco mine, Brazil. J. Mater. Res. Technol. 5, 339–344. https://doi.org/10.1016/j.jmrt.2016.03.008.

Islam, K., Murakami, S., 2021. Global-scale impact analysis of mine tailings dam failures: 1915–2020. Global Environ. Change 70. https://doi.org/10.1016/j.gloenvcha.2021.102361 102361.

Jefferies, M., 2022. On the fundamental nature of the state parameter. Géotechnique 72, 1082–1091. https://doi.org/10.1680/jgeot.20.P.228.

Jefferies, M., Shuttle, D.A., 2002. Dilatancy in General Cambridge-Type Models. Géotechnique 52, 625–638. https://doi.org/10.1680/geot.2002.52.9.625.

Kossoff, D., Dubbin, W.E., Alfredsson, M., Edwards, S.J., Macklin, M. G., Hudson-Edwards, K.A., 2014. Mine tailings dams: Characteristics, failure, environmental impacts, and remediation. Appl. Geochem. 51, 229–245. https://doi.org/10.1016/j.apgeochem.2014.09.010.

Kuhn, M.R., 2016. The critical state of granular media: Convergence, stationarity and disorder. Géotechnique 66, 902–909. https://doi.org/10.1680/jgeot.16.P.008.

Li, W., Coop, M.R., 2019. Mechanical behaviour of Panzhihua iron tailings. Can. Geotech. J. 56, 420–435. https://doi.org/10.1139/cgj-2018-0032.

Li, W., Coop, M.R., Senetakis, K., Schnaid, F., 2018. The mechanics of a silt-sized gold tailing. Eng. Geol. 241, 97–108. https://doi.org/10.1016/j.enggeo.2018.05.014.

Lupo, J.F., Hall, J.E., 2010. Dry stack tailings – design considerations. In: Tailings and Mine Waste'10. Edited by The Organizing Committee of the 14th International Conference on Tailings and Mine Waste. Taylor and Francis Group. ISBN 978-0-415-61455-9.

Perić, D., Ayari, M.A., 2002. Influence of Lode's angle on the pore pressure generation in soils. Int. J. Plasticity 18, 1039–1059. https://doi.org/10.1016/S0749-6419(01)00024-9.

Poorooshasb, H.B., 1989. Description of flow of sand using state parameters. Comput. Geotech. 8, 195–218. https://doi.org/10.1016/0266-352X(89)90043-8.

Selig, E., Ladd, R., 1978. Preparing test specimens using undercompaction. Geotech. Test. J. 1, 16. https://doi.org/10.1520/GTJ10364J.

Vaid, Y.P., Sasitharan, S., 1992. The strength and dilatancy of sand. Can. Geotech. J. 29, 522–526. https://doi.org/10.1139/t92-058.

Viana da Fonseca, A.V., Cordeiro, D., Molina-Gómez, F., 2021. Recommended procedures to assess critical state locus from triaxial tests in cohesionless remoulded samples. Geotechnics 1, 95–127. https://doi.org/10.3390/geotechnics1010006.

Viana da Fonseca, A., Cordeiro, D., Molina-Gómez, F., Besenzon, D., Fonseca, A., Ferreira, C., 2022. The mechanics of iron tailings from laboratory tests on reconstituted samples collected in post-mortem Dam I in Brumadinho. Soils & Rocks 45, 1–20. https://doi.org/10.28927/SR.2022.001122.

Wood, D.M., 2008. Critical state and soil modelling. In: Proceedings of the 4th International Symposium on Deformation Characteristics of Geomaterials, Millpress.

Xiaolong, Z., Shiyu, Z., Hui, L., Yingliang, Z., 2021. Disposal of mine tailings via geopolymerization. J. Cleaner Product. 284, 124756. https://doi.org/10.1016/j.jclepro.2020.124756.

Yang, Y., Wei, Z., Fourie, A., Chen, Y., Zheng, B., Wang, W., Zhuang, S., 2019. Particle shape analysis of tailings using digital image processing. Environ. Sci. Pollut. Res. 26, 26397–26403. https://doi.org/10.1007/s11356-019-05974-6.

Yao, C., Wu, L., Yang, J., Xiao, L., Liu, X., Jiang, Q., Zhou, C., 2021. Influences of tailings particle size on overtopping tailings dam failures. Mine Water Environ. 40, 174–188. https://doi.org/10.1007/s10230-020-00725-3.

Yin, G., Li, G., Wei, Z., Wan, L., Shui, G., Jing, X., 2011. Stability analysis of a copper tailings dam via laboratory model tests: a Chinese case study. Min. Eng. 24, 122–130. https://doi.org/10.1016/j.mineng.2010.10.014.